

Magnetic, thermal and transport properties of Cd doped CeIn₃

N. Berry,¹ E. M. Bittar,^{2,1} C. Capan,¹ P. G. Pagliuso,² and Z. Fisk¹

¹*Department of Physics and Astronomy,
University of California Irvine, Irvine, CA 92697-4575*

²*Instituto de Física “Gleb Wataghin”, UNICAMP,
C. P. 6165, 13083-970, Campinas, SP, Brazil*

(Dated: May 29, 2022)

Abstract

We have investigated the effect of Cd substitution on the archetypal heavy fermion antiferromagnet CeIn₃ via magnetic susceptibility, specific heat and resistivity measurements. The suppression of the Neel temperature, T_N , with Cd doping is more pronounced than with Sn. Nevertheless, a doping induced quantum critical point does not appear to be achievable in this system. The magnetic entropy at T_N and the temperature of the maximum in resistivity are also systematically suppressed with Cd, while the effective moment and the Curie-Weiss temperature in the paramagnetic state are not affected. These results suggest that Cd locally disrupts the AFM order on its neighboring Ce moments, without affecting the valence of Ce. Moreover, the temperature dependence of the specific heat below T_N is not consistent with 3D magnons in pure as well as in Cd-doped CeIn₃, a point that has been missed in previous investigations of CeIn₃ and that has bearing on the type of quantum criticality in this system.

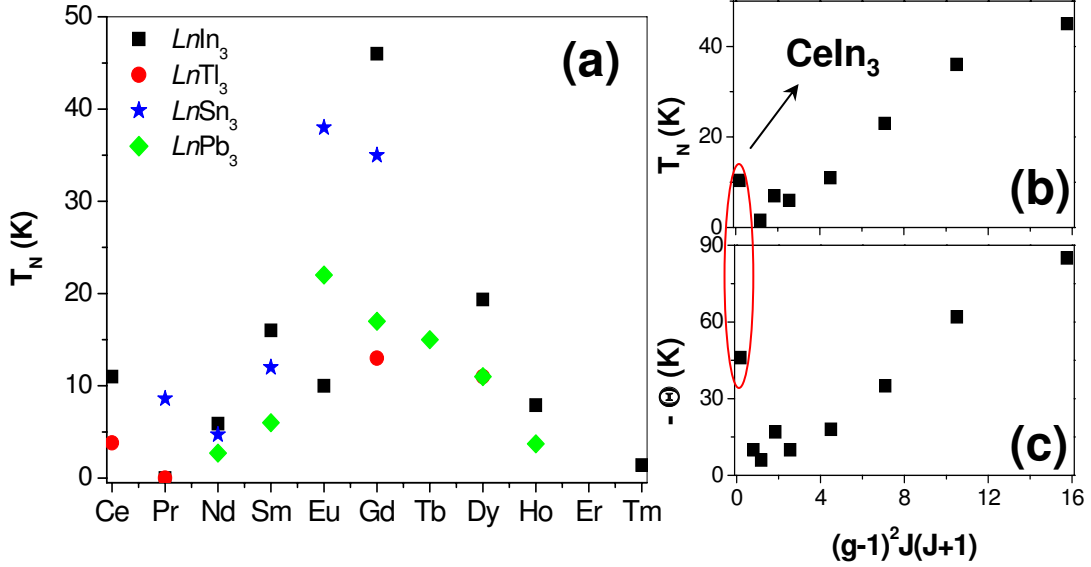


FIG. 1: (Color Online) (a) Neel temperature vs rare earth in $LnIn_3^1$, $LnTl_3$, $LnSn_3$ and $LnPb_3^7$. (b), (c) Neel temperature and Curie-Weiss temperature vs DeGennes factor $(g^2 - 1)^2 J(J + 1)$ in $LnIn_3^1$.

I. INTRODUCTION

CeIn₃ is a heavy fermion antiferromagnet (AFM) belonging to the family of Ce-binaries that form in the cubic Cu₃Au structure. Its Neel temperature $T_N = 10.2$ K is much larger than expected from a simple DeGennes scaling¹. Indeed both the Neel and the Curie-Weiss temperatures for CeIn₃ deviate from the DeGennes scaling, as seen in Fig. 1. The Curie-Weiss temperature in rare-earth compounds reflects the strength of the intersite (RKKY) coupling and thus should follow the DeGennes factor $(g^2 - 1)^2 J(J + 1)$. At low temperatures, the Kondo screening of Ce moments is expected to reduce rather than enhance the intersite coupling, so a larger T_N is quite surprising. In either case, this deviation might be attributed to crystal field effects. Note that the DeGennes scaling is well-obeyed in the related layered $CeMIn_5$ and Ce_2MIn_8 ($M = Co, Rh, Ir$) compounds². CeIn₃ also exhibits pressure-induced superconductivity, with $T_c^{max} = 0.2$ K, around the critical pressure where T_N is suppressed to zero^{3,4}. NQR measurements indicate homogeneous coexistence between superconductivity and the AFM state under pressure⁵. The occurrence of superconductivity in the vicinity of the AFM quantum critical point originally lead to the idea of magnetically mediated Cooper pairing in this and other heavy fermion superconductors^{3,6}.

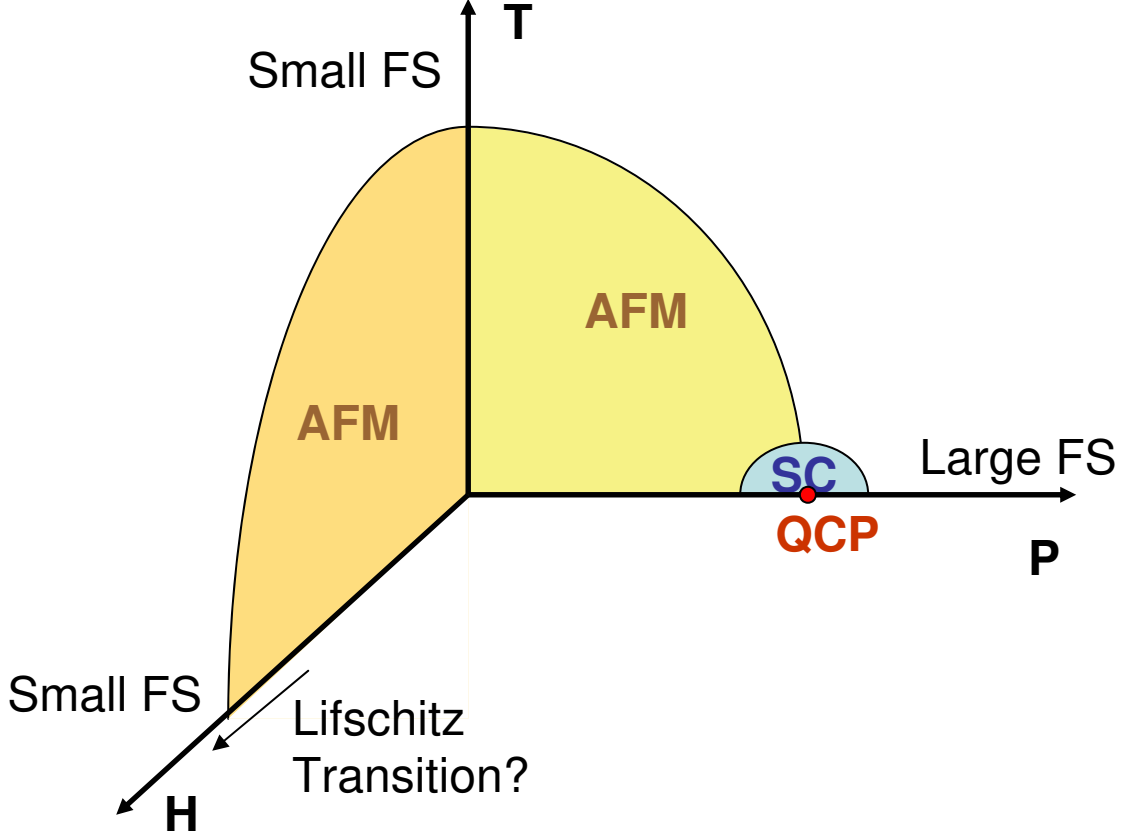


FIG. 2: (Color Online) Schematic temperature-pressure-magnetic field phase diagram of pure CeIn_3 .

CeIn_3 is one of the most thoroughly studied systems among heavy fermion compounds, in part due to the availability of large single crystals of high quality. Its magnetic structure and fluctuations are well characterized via neutron scattering^{8,9}, with a commensurate ordering wavevector of $(1/2, 1/2, 1/2)$ and an ordered moment of $\sim 0.6\mu_B$, close to the expected moment for the crystal field ground state, Γ_7 ¹⁰. Evidence for Kondo coupling has been found in resonant photoemission^{11,12}, in form of a broad peak at the Fermi level, similar to CeSn_3 but with a weaker hybridization, as well as in inelastic neutron scattering⁹, in form of a non-dispersive quasi-elastic peak corresponding to a single ion Kondo scale $T_K \sim 10$ K, of the same order as T_N . The magnetic entropy recovered at T_N is close to $RLn2$, meaning that the Kondo coupling does not efficiently quench the local moments prior to magnetic ordering. This is also supported by a moderately large electronic specific heat coefficient in the paramagnetic state, $\gamma \sim 180$ mJ/K²mol, corresponding to a mass enhancement of 27 compared to the non-magnetic La-analog.

The Fermi Surface (FS) of CeIn_3 continues to be a focus of attention, in connection with the theoretical possibility of a FS change across a zero temperature AFM instability, also called a quantum critical point (QCP)¹³. Hot spots have been identified in pulsed field dHvA measurements, with a divergent effective mass for field $B \parallel [111]$ ¹⁴. The corresponding region of the FS is the protruded neck in LaIn_3 and the mass enhancement has been attributed to the topological change due to the AFM Brillouin zone boundary crossing the FS¹⁵. The CeIn_3 Fermi surface has been mapped in the PM state via electron-positron annihilation technique and corresponds to fully localized $4f$ -electrons¹⁶. More recently it is claimed that the divergence of the effective mass actually happens within the Neel state, pointing to a FS topology change generically known as a Lifshitz transition¹⁷. Moreover, the field polarized PM state (for $B \geq B_c \sim 60$ T) has a small FS (corresponding to localized f -electrons) at ambient pressure¹⁸ but a large FS (corresponding to itinerant f -electrons) at high pressure (for $p \geq p_c$)¹⁹⁻²¹. The phase diagram of CeIn_3 is schematically represented in Fig 2. It is unclear how the FS continuously evolves from small to large in the PM state with applied pressure.

Evidence for a pressure induced QCP in the CeIn_3 phase diagram comes from the fact that the resistivity exhibits a temperature exponent strictly less than 2 at p_c , corresponding to a breakdown of the Fermi Liquid behavior⁴. The FS volume increase, deduced from dHvA under pressure¹⁹⁻²¹, across the critical pressure $p_c = 2.6 \text{ GPa}$ where AFM is suppressed, suggests a local QCP, where the f -electrons drop out of the FS when they order magnetically¹³. The commonly accepted examples of a local QCP are $\text{CeCu}_{5.9}\text{Au}_{0.1}$ ²² and YbRh_2Si_2 ²³. Doping studies of CeIn_3 , on the other hand, are more consistent with a spin-density wave type of QCP^{24,25}, where the f -electrons retain their localized character on both sides of the QCP. The AFM order in $\text{CeIn}_{3-x}\text{Sn}_x$ can be suppressed to $T = 0$ at $x_c \simeq 0.7$, with a logarithmically divergent electronic specific heat^{26,27}, characteristic of heavy fermion compounds at the QCP. The divergence of the Gruneisen ratio at this concentration has the exponent expected from a 3D-SDW QCP²⁸. This is also supported by the fact that there is no real breakdown of the FL behavior in the resistivity of a $x = 0.25$ sample when the Neel order is suppressed by a large applied magnetic field²⁹. An important open question is then: is there two distinct QCP's with different mechanisms in this system? if so, how are the two related in a pressure-doping phase diagram? The answer to such questions is likely to advance significantly our understanding of quantum

criticality in heavy fermion systems.

In this paper we report susceptibility, specific heat and resistivity measurements in Cd doped CeIn_3 . Cd substitution to In is equivalent to hole doping, as opposed to electron doping with Sn, which is known to induce a valence transition³⁰. Cd doping in the related CeMIn_5 ($M = \text{Co, Rh, Ir}$) has led to unexpected results, with a few percent Cd suppressing superconductivity in favor of the AFM state in both CeCoIn_5 and CeIrIn_5 , while the T_N in CeRhIn_5 has a non-monotonic evolution with doping³¹. Perhaps the most noteworthy aspect is that the effect of Cd doping can be reversed by applying pressure³¹, even though the lattice volume change due to Cd is minute. Also, NMR measurements in Cd doped CeCoIn_5 suggest that Cd enhances AFM correlations locally among the neighboring Ce ions³², and it remains a mystery how such antiferromagnetic droplets can percolate at the level of a few percent Cd introduced. These results have motivated us to investigate the effect of Cd in CeIn_3 and our main findings can be summarized as follows: Cd monotonically suppresses T_N , the magnetic entropy at T_N , as well as the paramagnetic electronic specific heat coefficient (γ_0) in CeIn_3 , without changing the Curie-Weiss behavior of Ce. This suggests that the valence of Ce is not affected by Cd, in the concentration range investigated. These results, very similar to the effect of Sn at low doping levels, mirrors the electron-hole symmetry in the system. The second important result is that the AFM magnon contribution to the heat capacity is not consistent with 3D magnon spectrum, a point that has been missed in previous reports. The possibility of 2D spin fluctuations makes it difficult to infer the type of quantum critical point in pure as well as Cd doped CeIn_3 based on dimensional analysis.

The paper is organized in four parts: in the first two sections we detail the crystal growth procedure and discuss the doping and magnetic field phase diagrams; in the following sections we present detailed analysis of resistivity and heat capacity measurements.

TABLE I: Characteristic parameters of $\text{Ce}(\text{In}_{1-x}\text{Cd}_x)_y$ single crystals: nominal (x_{nom}) concentration of Cd, effective composition x and y as determined from EDS, lattice constant a (\AA), Neel temperature $T_N(K)$, Curie-Weiss temperature $\Theta(K)$ and effective moment $\mu_{eff}(\mu_B)$. The concentrations noted with \dagger are from the two-step growth process.

x_{nom}	x	y	a	T_N	$-\Theta$	μ_{eff}
0	0	3	4.690	10.2	56.5	2.66
0.05	0.0198	2.63	4.690	9.5	50	2.70
0.1	0.0221	2.64	4.688	9.08	56.4	2.63
0.1 \dagger	0.0174	3	–	9.8	–	–
0.2	0.0295	2.62	4.687	8.15	52.8	2.63
0.2 \dagger	0.0223	3	–	9.6	–	–
0.3	0.0501	2.63	–	7.1	50.3	2.66
0.4	0.0740	2.59	4.686	6.71	49.3	2.64
0.4 \dagger	0.0199	3	–	9.15	–	–
0.5	0.121	2.59	4.691	6	56.5	2.66
0.5 \dagger	0.0199	3	–	9	–	–
0.6	0.0810	2.47	4.690	6.45	57.9	2.73
0.6 \dagger	0.0303	3	–	8.8	–	–

II. CRYSTAL GROWTH AND CHARACTERIZATION

Single crystals of $\text{Ce}(\text{In}_{1-x}\text{Cd}_x)_y$ were grown out of In:Cd flux with a starting molar ratio of 1:20(1-x):20x (Ce:In:Cd). Their characteristic parameters: composition, lattice constant, T_N and Curie-Weiss parameters are listed in Table I. Energy dispersive X-ray analysis (EDS) shows that these samples are off-stoichiometric in Indium with $y \simeq 2.6$ rather than 3. This corresponds to the surface (rather than the bulk) composition and appears to be the result of etching the samples in dilute HCl (in order to remove the excess In flux), since we find the correct Ce:In ratio in the un-etched pure compound grown on stoichiometry (1:3). From EDS, we determine the ratio of the effective versus the nominal Cd concentration to be 1:10, similar to the Cd doping of CeMIn_5 (M=Co,Rh,Ir). We have been unsuccessful in reaching Cd concentrations higher than effectively 12.1%. Since CeCd_3 does not crystallize

in the Cu_3Au structure, excessive Cd in the flux leads to secondary phases such as CeCd_{11} .

We have also attempted to grow more stoichiometric samples for resistivity measurements in a two-step process where we first pre-react Ce:Cd:In in desired proportions (solid state reaction at 1180 °C for 8 h in alumina crucible), followed by a second round in the furnace with excess In flux (1:10) in the crucible where we slowly cool (10 °C/h) from 1180 °C. The resulting crystals have a ratio of Ce to (In+Cd) very close to 1:3 but are overall more dilute in Cd than the first set of crystals. The EDS concentrations and T_N (determined from ρ) for these are also reported in Table I.

The Curie-Weiss parameters and the Neel temperatures reported in Table I are determined from the magnetic susceptibility (χ). Magnetization was measured at $H = 1$ T from 1.8 K to 400 K using a commercial vibrating sample SQUID magnetometer (Quantum Design). The inverse susceptibility, shown in Fig. 3a, is linear in temperature between 100 – 400 K for all dopings. The linear fits yield a Curie-Weiss moment (slope of χ^{-1}) μ_{eff} close to the theoretical value for Ce^{3+} ($2.54\mu_B$) and an antiferromagnetic Curie-Weiss temperature (T-axis intercept) $\Theta \simeq -50$ K, similar to the pure compound, with no systematic variation as a function of Cd concentration. The antiferromagnetic transition at T_N is marked by a peak in the susceptibility, as seen in Fig. 3b, and T_N is monotonically suppressed with Cd doping, as listed in Table I and also shown in figures 4a and 4b.

The monotonic decrease of T_N with increasing Cd concentration indicates that Cd effectively substitutes to In. However, no systematic evolution of the lattice constant a with doping is observed (see Table I). The lattice constants a have been determined from Rietveld refinement of powder X-ray diffraction spectra, using Si as a standard. One would expect the lattice to shrink with Cd, since Cd is smaller than In. A systematic suppression of a with Cd concentration was indeed observed in Cd doped CeCoIn_5 ³³. In addition, a increases systematically with Sn in CeIn_3 , as expected, Sn being larger than In³⁰.

In principle, Cd dopants could capture an electron from the conduction band, which would force the neighboring Ce^{3+} ion to give its f electron in order to ensure electric neutrality locally, thus becoming a non-magnetic Ce^{4+} ion. Since the concentration and

effective moment of Ce^{3+} ions in the PM state does not change with Cd, this can be effectively ruled out. Thus the Curie-Weiss analysis and the absence of change in the lattice constant rule out any valence change of Ce induced by Cd, in the doping range investigated. In comparison, it is known that with Sn doping the Ce^{3+} ions undergo a valence change, with CeSn_3 being in the (homogeneous) intermediate valence regime³⁰. In this case, the Curie-Weiss temperature shows a steep increase at the critical Sn concentration where the lattice constant exhibits a kink, corresponding to the intermediate valence regime³⁰.

Finally, the origin of the low temperature Curie tail in the susceptibility, observed only at low concentrations, as seen in Fig. 3b, is presently unknown and somewhat sample dependent. A similar upturn is also present in Sn-doped samples²⁷. We have also observed such upturns in some of the pure samples so it does not appear to be doping induced.

III. PHASE DIAGRAM

The suppression of T_N with Cd doping is surprising since Cd enhances T_N in the CeMIn_5 and Ce_2MIn_8 ($M = \text{Co, Rh, Ir}$) compounds^{31,34,35}. This difference may be due to the fact that in the tetragonal compounds there are two In sites and Cd preferentially substitutes to the in-plane In³³. It is instructive to compare the suppression of T_N in Cd and Sn doped samples, as shown in Fig. 4a. The values of T_N for Sn doped samples are from ref²⁷. The values of T_N in Cd doped CeIn_3 , determined from the peak in susceptibility, or the kink in the entropy and the resistivity, are in close agreement with one and other, as shown in figure 4b. Moreover, the consistency between the T_N values for the two set of samples, In deficient and stoichiometric, (see Table I) show that the surface depletion of In does not affect the bulk properties. For both dopants, Sn and Cd, T_N follows a $x^{-1/3}$ dependence, as shown in Fig. 4a, where $x^{-1/3}$ corresponds to the average distance between dopants. This suggests a similar mechanisms for the suppression of the AFM order. The weaker slope for Cd in Fig. 4a means a stronger suppression of T_N as compared to Sn. Nevertheless a doping induced QCP is unlikely in the case of Cd since the x-axis intercept is negative. In the doping range shown, neither Cd nor Sn changes the effective moment and Curie-Weiss temperature of Ce at high temperatures, thus it is likely that both Cd and Sn prevent their

Ce neighbors from ordering with respect to the local Weiss field below T_N . In other words, the AFM order is suppressed locally around the dopants rather than a global reduction of the RKKY coupling of Ce local moments.

Figure 4c shows the normalized H-T phase diagram of Cd doped CeIn₃, the data for the pure CeIn₃ is taken from ref.¹⁴. The H-T phase diagram is established from the heat capacity measurements at 0, 3 T, 6 T, 9 T for $x = 2.21\%$ and 12.1% samples. We have verified that the magnetic field suppression of T_N is independent of x provided we normalize T_N by $T_N(H = 0)$ and H by H_{max} , where H_{max} is defined as the critical field for the AFM transition at zero temperature ($T_N(H_{max}) = 0$). The value of $H_{max} = 60$ T is used for pure CeIn₃, consistently with Ref.¹⁴. Then H_{max} is adjusted for the Cd doped samples to give the best overlap in the normalized phase diagram. We find $H_{max} = 60$ T and 30 T for the $x = 2.21\%$ ($T_N = 9.075$ K) and 12.1% ($T_N = 6$ K) samples. The fact that reducing T_N by a factor of ~ 2 results in a suppression of H_{max} of the same rate suggests that the same effective moment μ_{eff} is involved in the Zeeman energy ($g\mu_{eff}H_{max} = k_B T_N$) for the 12.1% Cd doped sample as for the pure CeIn₃.

Thus, the (effective) ordered moment per Ce within the AFM state does not change with Cd, based on the H-T phase diagram. This suggests that the CEF ground state does not change with Cd. One is then lead to speculate that the number of Ce³⁺ ions participating in the Neel order is decreasing with increasing Cd concentration, possibly as a result of local disruption caused by doping, as discussed above. However, this cannot solely explain the suppression of the AFM state since it is hard to reconcile a local scenario with a simultaneous decrease of the magnetic entropy at T_N (see below). The investigation of the magnetic fluctuations in the vicinity of Cd in CeIn₃ with NMR, of the local structure of Ce by EXAFS as well as the investigation of possible changes in the magnetic structure via neutron scattering will likely shed more light on the mechanism of suppression of the AFM order with Cd.

IV. HEAT CAPACITY

A. The magnetic entropy at T_N

Figure 5a shows the temperature dependence of the total specific heat (C) down to 0.5 K in single crystals of $\text{Ce}(\text{In}_{1-x}\text{Cd}_x)_{2.6}$ at zero magnetic field, for the indicated nominal concentrations. The non-magnetic analog, LaIn_3 is also measured in order to estimate and subtract the lattice contribution (see fig 5a). The AFM transition is marked by a jump in C , characteristic of a second order transition. The corresponding magnetic entropy $S_{mag}(T_N) = \int^{T_N} \frac{C-C_{latt}}{T} dT$ is obtained by integrating the magnetic contribution to specific heat up to T_N , and shown as a function of T_N in Fig. 4d. S_{mag} decreases monotonically with doping.

The size of the specific heat jump is surprisingly non-monotonic as a function of Cd concentration: it first decreases from 0 to 2.23%Cd and then increases from 2.23 to 12.1%Cd. This may correspond to the AFM transition evolving from a second order to a weakly first order one, although the susceptibility anomaly nor the drop in the entropy $S(T)$ at T_N become discontinuous. Further investigations of the sublattice magnetization or the magneto-caloric effect are needed to address this issue.

The local suppression of the AFM around the Cd impurities, as suggested above, cannot alone be responsible for the observed entropy loss upon Cd doping. Rather, it may be due to a more effective Kondo screening prior to ordering: if T_N decreases faster than T_K , the magnetic entropy at the transition will be suppressed simply because of the quenching of Ce moments. We have determined the single-ion Kondo temperature T_K of $\text{La}_{0.95}\text{Ce}_{0.05}\text{In}_3$ doped with 10% nominal Cd (2% effective) from specific heat (not shown) and found that the magnetic entropy reaches $\frac{1}{2}R\ln 2$ at $T_K = 11$ K, which corresponds to the same single-ion Kondo temperature as in pure CeIn_3 ⁹. Therefore Cd has very little effect on T_K while it suppresses T_N monotonically. The screening of the Ce moments for $T_N \leq T \leq T_K$ results in a lower entropy at T_N .

B. The electronic specific heat coefficient

The electronic specific heat coefficient γ_0 in the PM state is obtained from linear fits to $\frac{C}{T}$ vs T^2 in the range 11 – 20 K. The linearity of $\frac{C}{T}$ vs T^2 for all Cd concentrations, as seen

in Fig. 5b, suggests that any additional contribution to heat capacity (from CEF excitations or AFM fluctuations) is negligible in this range. The slight increase in the slope of $\frac{C}{T}$ vs T^2 with increasing Cd concentration results in a suppression of the T=0 intercept, which defines γ_0 . The error bars on γ_0 comes from the choice of the temperature range used in fitting. Within the error bars, γ_0 is suppressed with increasing Cd concentration, as shown in Fig. 4d.

The simultaneous suppression of the magnetic order and the heavy fermion state is at odds with the Doniach phase diagram, where a heavy paramagnetic state emerges beyond the critical point where the AFM state is suppressed. Since the γ_0 is determined at temperatures nominally higher than T_K , it may not properly reflect the mass renormalization occurring at the lowest temperatures (within the AFM state). Nevertheless the γ_0 in the AFM state also appears to decrease with increased doping, as seen in Fig. 5d, so that our data effectively rules out any mass enhancement concomitant with the suppression of T_N .

C. AFM magnon contribution

Figure 5c and 5d show the magnetic part of the specific heat, in the AFM state ($T < T_N$), obtained by subtracting the lattice contribution. At low temperatures, antiferromagnetic magnon contribution is expected to follow a T^3 law in 3D³⁶. This is because the AFM magnon dispersion is to a good approximation linear in an intermediate temperature range and the calculation of heat capacity follows by analogy with the Debye model. The comparison of C_{mag} vs T^2 (Fig. 5c) and $\frac{C_{mag}}{T}$ vs T^2 (Fig. 5d) reveals that the data are more consistent with a quadratic (T^2) behavior rather than cubic (T^3). In fact, the data collapse on a single curve at low T for all Cd concentrations in Fig. 5c, whereas there is no substantial T-range where $\frac{C_{mag}}{T}$ is linear in T^2 in Fig. 5d.

This unusual power law is clear evidence that the spin fluctuations in pure as well as Cd doped CeIn₃ are not 3D, contrary to what is commonly assumed for this cubic compound²⁸. Given the ordering wavevector, one possibility is that these are transverse spin fluctuations within the [111] planes and the system is effectively quasi-two dimensional. Future theoretical work, as well as a direct investigation of magnon spectrum via inelastic neutron scattering is strongly needed to address the origin of the T^2 behavior of the heat

capacity in the AFM state.

Two-dimensional fluctuations are not uncommon in the context of local quantum criticality and they have been observed in particular in $\text{CeCu}_{5.9}\text{Au}_{0.1}$ via inelastic neutron scattering measurements³⁷. We have checked with previously published data³⁸ that the specific heat of CeCu_5Au in the AFM state is also quadratic in temperature up to 0.5 K, consistently with CeIn_3 . This gives further evidence that in both systems the underlying physics involves 2D magnons. This suggests that one can effectively analyze the specific heat in the AFM state away from the QCP, to gain insight into the dimensionality of the spin fluctuations in other quantum critical systems as well. One immediate consequence of 2D spin fluctuations is that the sum of the physical dimension ($d = 2$) and the dynamical critical exponent ($z = 2$) is exactly 4, which is the upper critical dimension in the context of spin fluctuation theory^{24,25}. In other words, a wide fluctuation regime is possible in this system, so the dimensional analysis¹³ alone is not sufficient to distinguish between the SDW theory and the local QCP scenario in this case. Then Cd doped CeIn_3 is a potential candidate for FS volume change across the (pressure induced) QCP, just as the pure compound.

In summary, the main effect of Cd on the specific heat is: (i) an entropy loss at the transition, (ii) a suppression of the electronic specific heat coefficient γ_0 in the PM state. While the former can be understood in terms of an increased Kondo screening, the latter appears to contradict the Doniach phase diagram. Therefore it is unlikely that Cd doping itself tunes the system towards a QCP. Nevertheless, it is a sensible assumption that pressure will tune $\text{Ce}(\text{In,Cd})_3$ towards a QCP. Based on the anomalous (quadratic) behavior of the magnon heat capacity, we speculate that the magnetic fluctuations in this system are effectively 2D, which makes it impractical to determine the type of QCP from dimensional analysis.

V. RESISTIVITY

A. Coherence temperature

The temperature dependence of the magnetic part of the resistivity is shown on a semi-log plot for the two sets of Cd doped crystals, the In deficient and the stoichiometric ones, in Fig. 6a and Fig. 7a respectively. The resistivity was measured with the standard four-wire technique in the range 1.8 – 350 K, with Pt wires attached to the samples using silver paint. A current of 2 mA was applied. For the stoichiometric samples ($y = 3$), a modest field of 500 G was applied in order to suppress the superconducting transition of free In inclusions. The magnetic contribution ρ_{mag} is obtained by subtracting the phonon contribution from the total resistivity, assuming it is the same as for the LaIn_3 analog:

$$\rho_{mag} = \rho - \rho_{\text{LaIn}_3}.$$

The characteristic peak in $\rho_{mag}(T)$ is observed at $T_{max} = 50$ K in pure CeIn_3 , consistent with previous reports^{4,39}. It is also known that the peak in ρ in pure CeIn_3 is accompanied by a Schottky peak in the specific heat at around the same temperature⁴⁰. This Schottky peak is associated with a CEF excitation of $\simeq 10\text{meV}$, also seen in inelastic neutron scattering^{8,10}. T_{max} is usually taken as a crossover (or coherence) temperature from single ion to dense Kondo regime in heavy fermions⁴¹. It also corresponds to the crossover from a Kondo effect involving the full degeneracy of the $J = 5/2$ multiplet of the Ce^{3+} ion at high T to a Kondo effect restricted to the crystal field ground state at low T ⁴². The emerging picture from these two approaches is that the Kondo lattice coherence among Ce's is only achieved when the f -electrons condense into their CEF ground state. This is also consistent with the view that the T_{max} sets the scale of intersite coupling among Ce's, a conclusion reached in the La dilution study of CeCoIn_5 ⁴³.

In the present case, T_{max} is determined graphically for all Cd concentrations from the broad peak observed in resistivity, as shown by the arrows in Fig. 6a and 7a. When plotted against T_N , as done in Fig. 6c and 7c, one can see that T_{max} tends to decrease with decreasing T_N , due to Cd doping. A similar suppression of T_{max} is observed in Sn-doped CeIn_3 ²⁷. Note, however, that T_{max} is enhanced with Sn doping in CeCoIn_5 ⁴⁴, highlighting the different response of the tetragonal and cubic systems to the same dopant. The disorder

suppression of the Kondo coherence temperature in this and other heavy fermion systems is currently an open issue but it likely involves crystal field effects.

B. Resistivity upturn

The most striking change induced by Cd is a clear upturn in $\rho_{mag}(T)$ for $T_N \leq T \leq T_{max}$, as seen in Fig. 6a in In-deficient samples, $\text{Ce}(\text{In}_{1-x}\text{Cd}_x)_{2.6}$. The upturn becomes systematically more pronounced with increasing Cd concentrations. Moreover, the application of $H = 9$ T magnetic field does not suppress the upturn significantly (not shown). The stoichiometric compounds (Fig. 7a) do not show any upturn, but this could be simply because they are actually more dilute in Cd than their In-deficient counterparts. Thus, In deficiency alone does not appear to be the spurious cause of the upturn. A similar upturn is also reported in La-doped CeIn_3 ³⁹ as well as in other heavy fermion systems such as Ga doped CeAl_2 ⁴⁵. In the latter, it has been associated with a second Kondo scale. To the best of our knowledge, such an upturn is not found in Sn doped CeIn_3 , nor in any Cd doped CeMIn_5 ($M=\text{Co,Rh,Ir}$). Given the observed trends, and given the absence of the upturn in the pure compound, it is unlikely associated with a lower Kondo scale in Cd doped CeIn_3 . We are thus compelled to interpret it as a disorder effect associated with Cd doping.

C. Spin-disorder scattering

The onset of the antiferromagnetic transition at T_N is marked by a pronounced drop in $\rho(T)$ in all Cd doped samples (see arrows in Fig. 6a and 7a), corresponding to the suppression of spin-disorder scattering. In most rare-earth intermetallics exhibiting AFM ordering, the spin-disorder scattering in ρ , as well as the ordering temperature T_N , are proportional to the so-called DeGennes factor $(g^2 - 1)^2 J(J + 1)$, since both depend on the exchange coupling strength⁴⁶. Moreover, the derivative of ρ , $\frac{\partial \rho}{\partial T}$ is known to mimic the jump in the specific heat in a magnetic transition⁴⁷, and this is indeed the case in CeIn_3 ⁴.

In the present compounds, we found a non-monotonic evolution with Cd of the relative change in ρ_{mag} across T_N , namely the ratio $\frac{\Delta \rho_{mag}}{\rho_0}$. This ratio is defined as $\frac{\Delta \rho_{mag}}{\rho_0} = \frac{\rho(T_N) - \rho_0}{\rho_0}$,

with $\rho(T_N)$ the value of ρ_{mag} at T_N , and with ρ_0 , the residual resistivity, obtained from the quadratic fits (see below). As shown in the semi-log plot of Fig. 8c, $\frac{\Delta\rho_{mag}}{\rho_0}$ steeply decreases upon doping, with decreasing T_N , then saturates and slightly increases at higher Cd concentrations. The latter might be a consequence of the upturn in $\rho_{mag}(T)$ reported above. The initial sharp drop of $\frac{\Delta\rho_{mag}}{\rho_0}$ reflects the decreasing magnetic entropy upon doping, as expected from $\frac{\partial\rho}{\partial T} \propto C$. This is also consistent with the pressure results⁴, where the resistivity anomaly is suppressed together with T_N .

D. Fermi Liquid analysis

The temperature dependence of ρ_{mag} below T_N is quadratic in the pure as well as in most of the Cd doped CeIn₃ samples, as shown in Fig. 6b and 7b. The notable exceptions are the nominal 40% and 60% stoichiometric samples, which exhibit a pronounced negative curvature. The quadratic behavior of ρ_{mag} is consistent with a Fermi Liquid regime extending up to $T \simeq \frac{T_N}{2}$, also in agreement with previous reports⁴.

The observation of a T^2 resistivity on a wide T-range within the magnetically ordered state is unusual and implies a negligible electron-magnon scattering, as compared to the electron-electron scattering. The quadratic fits to $\rho_{mag} = \rho_0 + AT^2$ in both the In-deficient and stoichiometric samples, yield a Fermi Liquid coefficient A and residual resistivity ρ_0 , both of which are shown as a function of T_N on Fig. 8a and 8b. The systematic increase in ρ_0 with decreasing T_N (increasing Cd doping) is simply the expected impurity scattering from Cd. The corresponding increase in the A coefficient would in principle correspond to a mass enhancement.

At first, this is surprising since the Sommerfeld coefficient γ_0 both in the PM and the AFM states decreases with increasing Cd concentration. In most heavy fermions, as first noted by Kadowaki and Woods⁴⁸, the A coefficient of resistivity scales with the electronic specific heat coefficient. Therefore the thermodynamic results cast doubts on the validity of the interpretation of the quadratic behavior of resistivity in the AFM state in terms of Fermi Liquid behavior and of the evolution of the A coefficient with doping in terms of mass enhancement in Ce(In,Cd)₃.

In summary, the effect of Cd on the resistivity is complex. The suppression of the coherence temperature and the increase in the residual resistivity appear to be disorder related. The smaller spin-disorder scattering with increasing Cd concentration can be attributed to the loss of magnetic entropy at the transition. There is an unusual upturn induced by Cd, whose origin remains to be elucidated. The quadratic behavior of resistivity in the AFM state may be analyzed in terms of Fermi liquid behavior, as was previously done in pure CeIn₃, however the enhancement of the A coefficient is at odds with the simultaneous suppression of γ_0 with increasing Cd concentrations.

VI. CONCLUSION

In conclusion, susceptibility and resistivity measurements in Ce(In_{1-x}Cd_x)₃ consistently show that the Cd-suppression of the AFM state is not accompanied by any change of the Ce local moments, suggesting that Cd locally disrupts the long range order. The Sommerfeld coefficient is systematically and significantly suppressed in the PM state, suggesting a Cd induced suppression of the effective mass of carriers. The simultaneous suppression of the magnetic order and the heavy fermion state is at odds with the Doniach phase diagram and suggests that Cd tunes the system away from the QCP. The most striking effect of Cd in the PM state is the upturn seen in the resistivity, whose origin is currently unknown. In the AFM state, the Fermi liquid coefficient, determined from the resistivity, increases systematically with increasing Cd, which would in principle imply a mass enhancement. However, the concomitant increase in the residual resistivity as well as the presence of magnon scattering makes this interpretation dubious. Moreover, we found that the magnetic contribution to the specific heat has a T^2 behavior in the AFM state, inconsistent with 3D magnons. The reduced dimension for magnetic excitations, which is the likely origin of this quadratic behavior, have been missed in previous studies, and makes it difficult to assess the type of quantum criticality observed in this system based on dimensional analysis.

Acknowledgments

Z.F. acknowledges support through NSF Grant No. NSF-DMR-0503361. E.M.B. and P.G.P. acknowledge support through CNPq (grant No. 200563/2008-4) and FAPESP (grant No. 2006/55347-1).

- ¹ K. H. J. Buschow, H. W. de Wijn, and A. M. van Diepen, *The Journal of Chemical Physics* **50**, 137 (1969).
- ² P. G. Pagliuso, J. D. Thompson, M. F. Hundley, J. L. Sarrao, and Z. Fisk, *Phys. Rev. B* **63**, 054426 (2001).
- ³ N. D. Mathur, F. M. Grosche, S. R. Julian, I. R. Walker, D. M. Freye, R. K. W. Haselwimmer, and G. G. Lonzarich, *Nature* **394**, 39 (1998).
- ⁴ G. Knebel, D. Braithwaite, P. C. Canfield, G. Lapertot, and J. Flouquet, *Phys. Rev. B* **65**, 024425 (2001).
- ⁵ S. Kawasaki, M. Yashima, Y. Kitaoka, K. Takeda, K. Shimizu, Y. Oishi, M. Takata, T. C. Kobayashi, H. Harima, S. Araki, et al., *Physical Review B* **77**, 064508 (2008).
- ⁶ P. Monthoux, D. Pines, and G. G. Lonzarich, *Nature* **450**, 1177 (2007).
- ⁷ K. H. J. Buschow, *Rep. Prog. Phys.* **42** (1979).
- ⁸ J. M. Lawrence and S. M. Shapiro, *Phys. Rev. B* **22**, 4379 (1980).
- ⁹ W. Knafo, S. Raymond, B. Fak, G. Lapertot, P. C. Canfield, and J. Flouquet, *J. Phys. Condens. Matter* **15**, 3741 (2003).
- ¹⁰ J. Boucherle, J. Flouquet, Y. Lassailly, J. Palleau, and J. Schweizer, *Journal of Magnetism and Magnetic Materials* **31-34**, 409 (1983).
- ¹¹ J. W. Allen, S. J. Oh, I. Lindau, J. M. Lawrence, L. I. Johansson, and S. B. Hagström, *Phys. Rev. Lett.* **46**, 1100 (1981).
- ¹² H.-D. Kim, O. Tjernberg, G. Chiaia, H. Kumigashira, T. Takahashi, L. Duò, O. Sakai, M. Kasaya, and I. Lindau, *Phys. Rev. B* **56**, 1620 (1997).
- ¹³ P. Coleman, C. Pepin, Q. Si, and R. Ramazashvili, *Journal of Physics: Condensed Matter* **13**, R723 (2001).
- ¹⁴ T. Ebihara, N. Harrison, M. Jaime, S. Uji, and J. C. Lashley, *Phys. Rev. Lett.* **93**, 246401

- (2004).
- ¹⁵ L. P. Gor'kov and P. D. Grigoriev, *Physical Review B* **73**, 060401(R) (2006).
 - ¹⁶ M. Biasini, G. Ferro, and A. Czopnik, *Phys. Rev. B* **68**, 094513 (2003).
 - ¹⁷ S. E. Sebastian, N. Harrison, C. D. Batista, S. A. Trugman, V. Fanelli, M. Jaime, T. P. Murphy, E. C. Palm, H. Harima, and T. Ebihara, arXiv:0902.4108v2 (2009).
 - ¹⁸ N. Harrison, S. E. Sebastian, C. H. Mielke, A. Paris, M. J. Gordon, C. A. Swenson, D. G. Rickel, M. D. Pacheco, P. F. Ruminer, J. B. Schillig, et al., *Physical Review Letters* **99**, 056401 (2007).
 - ¹⁹ R. Settai, T. Kubo, T. Matsuda, Y. Haga, Y. Onuki, and H. Harima, *Physica B: Condensed Matter* **378-380**, 417 (2006).
 - ²⁰ M. Endo, N. Kimura, H. Aoki, T. Terashima, S. Uji, T. Matsumoto, and T. Ebihara, *Phys. Rev. Lett.* **93**, 247003 (2004).
 - ²¹ R. Settai, T. Kubo, T. Shiromoto, D. Honda, H. Shishido, K. Sugiyama, Y. Haga, T. D. Matsuda, K. Betsuyaku, H. Harima, et al., *Journal of the Physical Society of Japan* **74**, 3016 (2005).
 - ²² A. Schroder, G. Aeppli, R. Coldea, M. Adams, O. Stockert, H. Lohneysen, E. Bucher, R. Ramazashvili, and P. Coleman, *Nature* **407**, 351 (2000).
 - ²³ P. Gegenwart, J. Custers, C. Geibel, K. Neumaier, T. Tayama, K. Tenya, O. Trovarelli, and F. Steglich, *Phys. Rev. Lett.* **89**, 056402 (2002).
 - ²⁴ J. A. Hertz, *Phys. Rev. B* **14**, 1165 (1976).
 - ²⁵ A. J. Millis, *Phys. Rev. B* **48**, 7183 (1993).
 - ²⁶ T. Rus, H. Wilhelm, O. Stockert, T. Lhmann, N. Caroca-Canales, J. Sereni, C. Geibel, and F. Steglich, *Physica B: Condensed Matter* **359-361**, 62 (2005).
 - ²⁷ P. Pedrazzini, M. G. Berisso, N. Caroca-Canales, M. Deppe, C. Geibel, and J. G. Sereni, *European Physical Journal B* **38**, 445 (2004).
 - ²⁸ R. Kuchler, P. Gegenwart, J. Custers, O. Stockert, N. Caroca-Canales, C. Geibel, J. G. Sereni, and F. Steglich, *Physical Review Letters* **96**, 256403 (2006).
 - ²⁹ A. V. Silhanek, T. Ebihara, N. Harrison, M. Jaime, K. Tezuka, V. Fanelli, and C. D. Batista, *Physical Review Letters* **96**, 206401 (2006).
 - ³⁰ J. Lawrence, *Phys. Rev. B* **20**, 3770 (1979).
 - ³¹ L. D. Pham, T. Park, S. Maquilon, J. D. Thompson, and Z. Fisk, *Physical Review Letters* **97**, 056404 (2006).

- ³² R. R. Urbano, B.-L. Young, N. J. Curro, J. D. Thompson, L. D. Pham, and Z. Fisk, *Physical Review Letters* **99**, 146402 (2007).
- ³³ C. H. Booth, E. D. Bauer, A. D. Bianchi, F. Ronning, J. D. Thompson, J. L. Sarrao, J. Y. Cho, J. Y. Chan, C. Capan, and Z. Fisk, *Physical Review B* **79**, 144519 (2009).
- ³⁴ C. Adriano, C. Giles, L. Mendonca-Ferreira, F. de Bergevin, C. Mazzoli, L. Paolasini, Z. Fisk, and P. G. Pagliuso, *Physica B* **404**, 3014 (2009).
- ³⁵ C. Adriano, C. Giles, E. M. Bittar, L. N. Coelho, F. de Bergevin, C. Mazzoli, L. Paolasini, W. Ratcliff, R. Bindel, J. W. Lynn, et al., arXiv.org:0912.4467 (2009).
- ³⁶ C. Kittel, *Quantum theory of solids*, John Wiley and Sons (1963).
- ³⁷ O. Stockert, H. v. Lohneysen, A. Rosch, N. Pyka, and M. Loewenhaupt, *Phys. Rev. Lett.* **80**, 5627 (1998).
- ³⁸ C. Paschke, C. Speck, G. Portisch, and H. v. Lohneysen, *J. Low Temp. Physics* **97**, 229 (1994).
- ³⁹ R. Elenbaas, C. Schinkel, and C. van Deudekom, *Journal of Magnetism and Magnetic Materials* **15-18**, 979 (1980).
- ⁴⁰ A. V. Diepen, R. Craig, and W. Wallage, *Journal of Physics and Chemistry of Solids* **32**, 1867 (1971).
- ⁴¹ M. Lavagna, C. Lacroix, and M. Cyrot, *Journal of Physics F: Metal Physics* **12**, 745 (1982).
- ⁴² B. Cornut and B. Coqblin, *Phys. Rev. B* **5**, 4541 (1972).
- ⁴³ S. Nakatsuji, S. Yeo, L. Balicas, Z. Fisk, P. Schlottmann, P. G. Pagliuso, N. O. Moreno, J. L. Sarrao, and J. D. Thompson, *Phys. Rev. Lett.* **89**, 106402 (2002).
- ⁴⁴ E. D. Bauer, F. Ronning, C. Capan, M. J. Graf, D. Vandervelde, H. Q. Yuan, M. B. Salamon, D. J. Mixson, N. O. Moreno, S. R. Brown, et al., *Physical Review B (Condensed Matter and Materials Physics)* **73**, 245109 (2006).
- ⁴⁵ A. Y. Takeuchi and S. F. da Cunha, *Journal of Alloys and Compounds* **226**, 126 (1995).
- ⁴⁶ J. Jensen and A. R. Mackintosh, *Rare Earth Magnetism: Structure and Excitations*, Clarendon Press, Oxford (1991).
- ⁴⁷ M. E. Fisher and J. S. Langer, *Phys. Rev. Lett.* **20** (1968).
- ⁴⁸ K. Kadowaki and S. B. Woods, *Solid State Communications* **58**, 507 (1986).

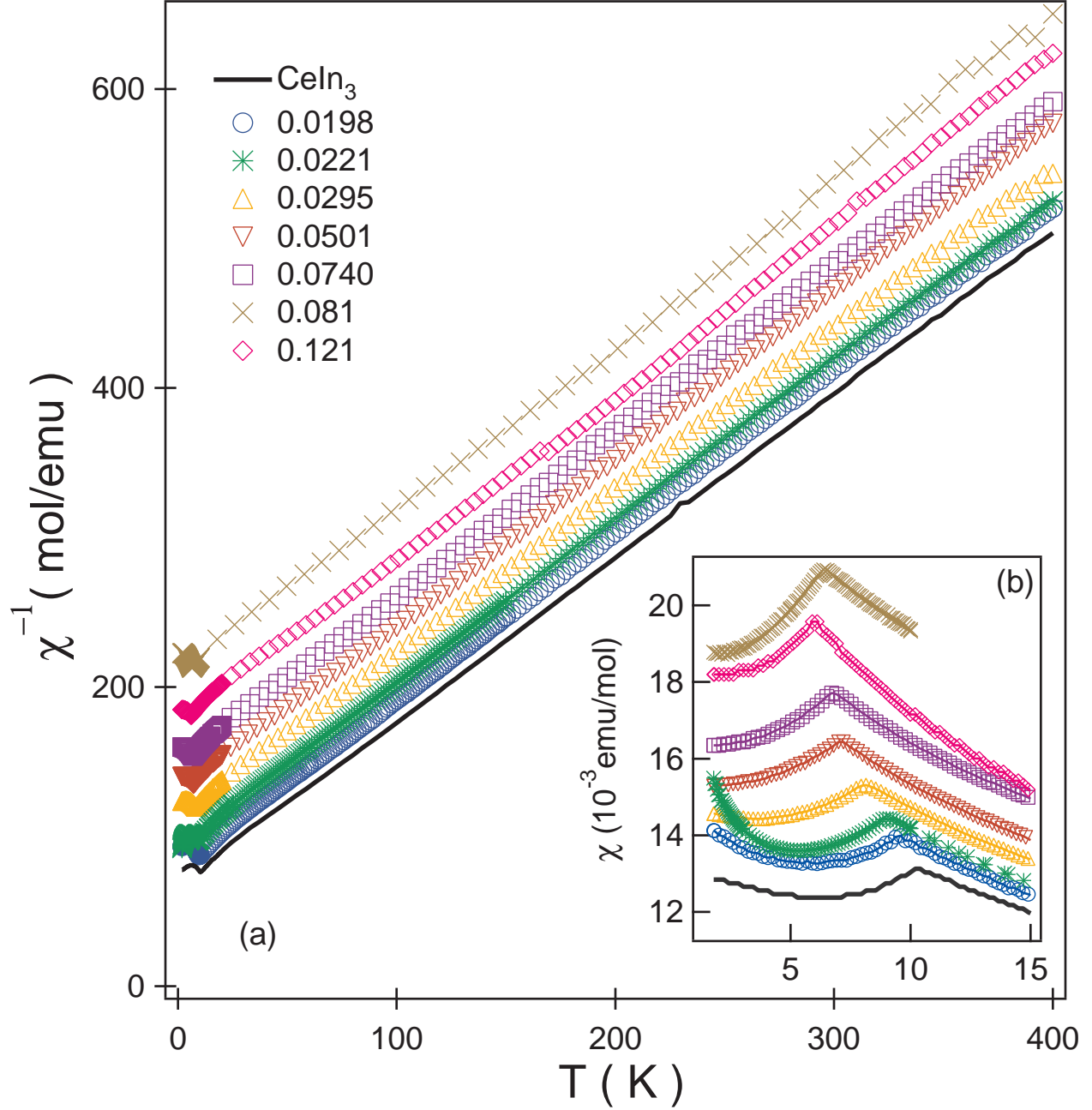


FIG. 3: (Color Online) (a) Inverse magnetic susceptibility (χ^{-1}) vs Temperature in $\text{Ce}(\text{In}_{1-x}\text{Cd}_x)_{2.6}$ single crystals. The data have been shifted vertically for clarity. The Cd concentrations as determined from EDS are indicated. (b) Susceptibility vs Temperature for the same samples below $T = 15$ K showing a maximum at the Neel temperature.

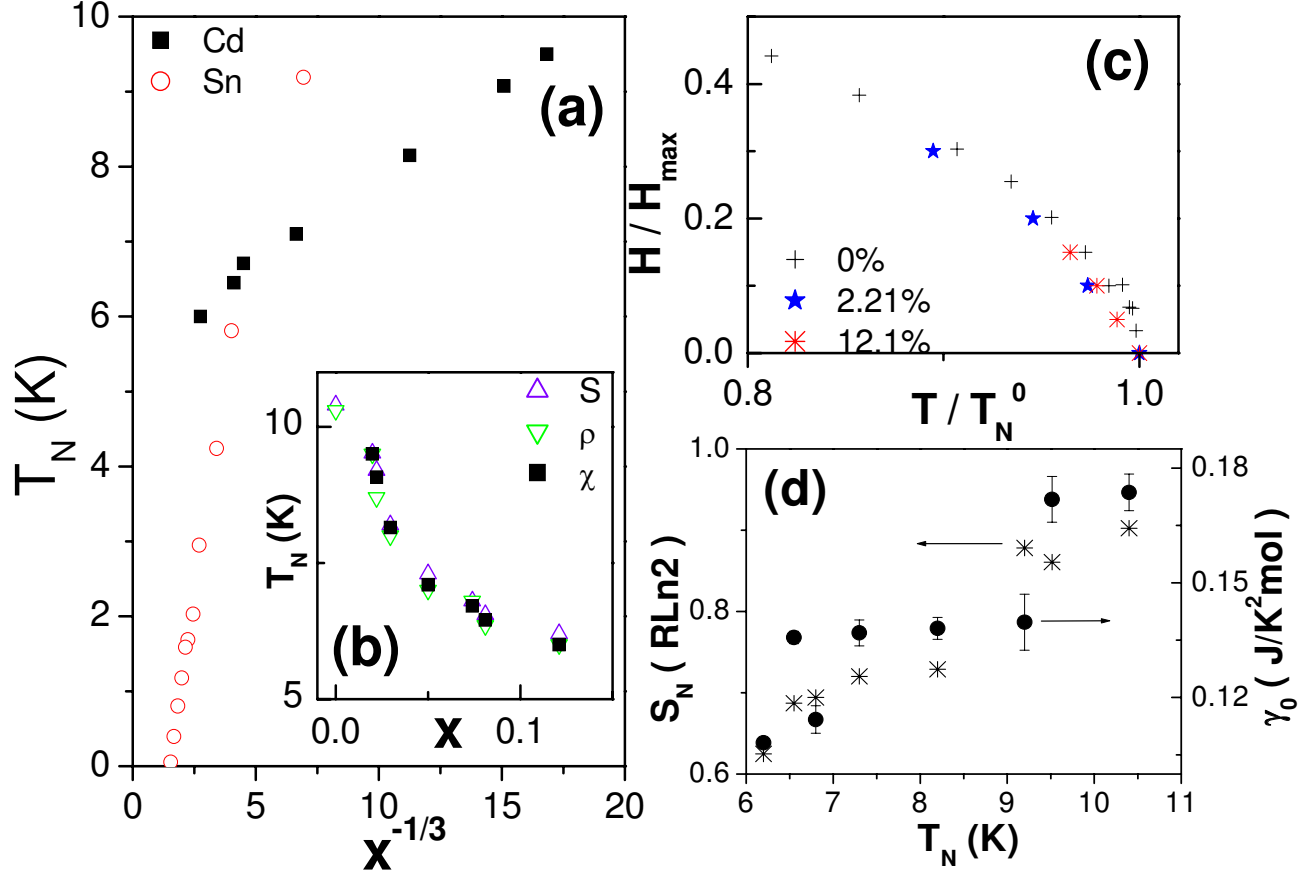


FIG. 4: (Color Online) (a) Neel Temperature (T_N) vs $x^{-1/3}$ in Sn and Cd doped CeIn₃. The values for Sn doping is taken from ref.²⁷. $x^{-1/3}$ represents the average distance between two dopant ions. For Cd, the effective concentrations are used, as determined from EDS. (b) Comparison of T_N , determined from different measurements, vs effective doping x in Ce(In_{1-x}Cd_x)_{2.6}. T_N is determined from the kink in the entropy (S), the kink in the resistivity (ρ) and the maximum in the magnetic susceptibility (χ). (c) Normalized H-T phase diagram of Ce(In_{1-x}Cd_x)_{2.6} for $x = 0$ (+), 2.21% (*) and 12.1% (*). The data for pure CeIn₃ is from ref.¹⁴. (d) Magnetic entropy recovered at T_N , S_N (*) and electronic specific heat coefficient in the PM state, γ_0 (•) vs Neel temperature, T_N in Ce(In_{1-x}Cd_x)_{2.6}.

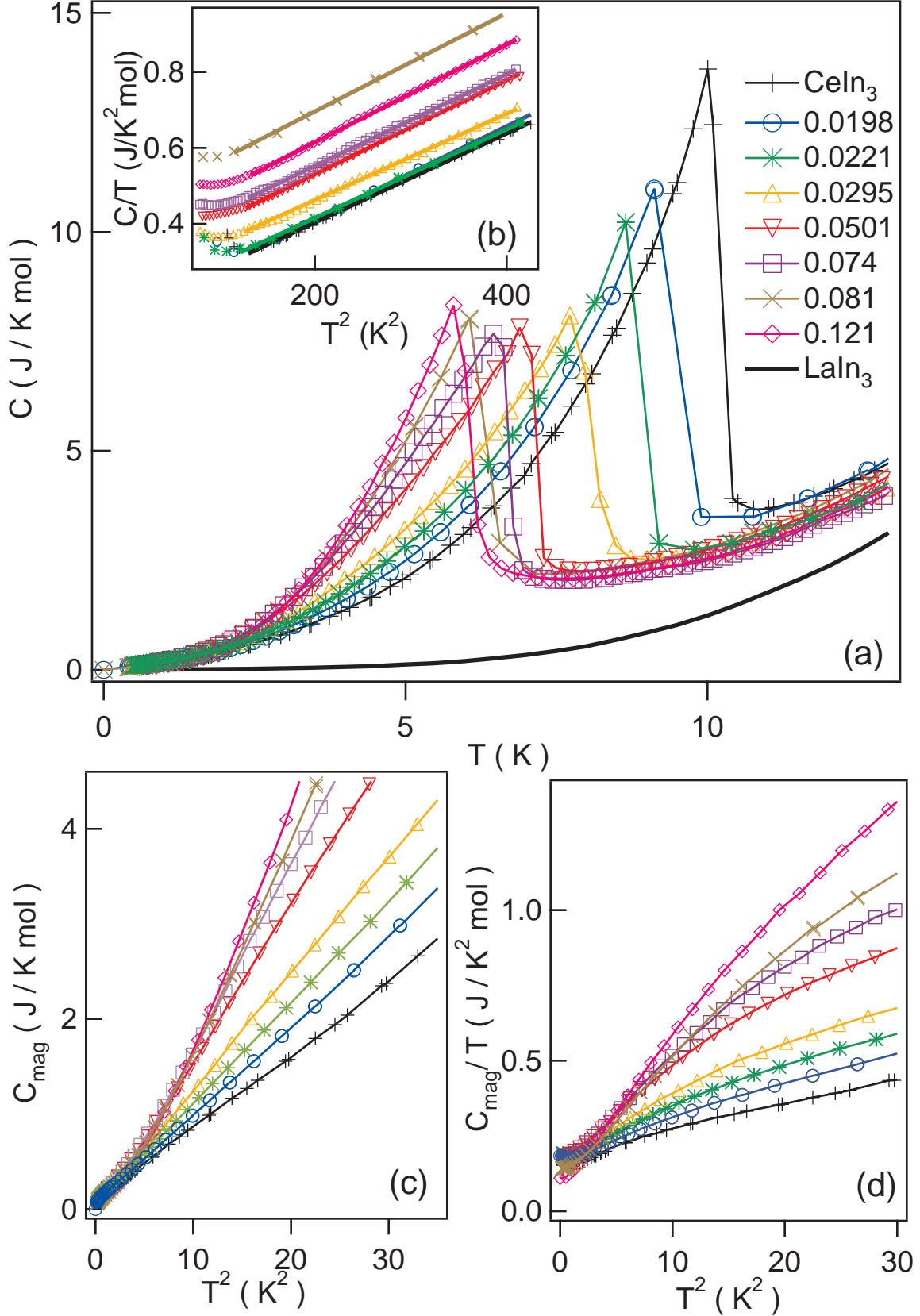


FIG. 5: (Color Online) (a) Total specific heat vs Temperature in single crystals of $\text{Ce}(\text{In}_{1-x}\text{Cd}_x)_{2.6}$, in the temperature range 0.5 – 15 K, at zero magnetic field. The Cd concentrations as determined from EDS are indicated. Also shown is the heat capacity of the non-magnetic LaIn_3 . (b) Specific heat divided by temperature (C/T) vs Temperature squared (T^2) in the paramagnetic state for the

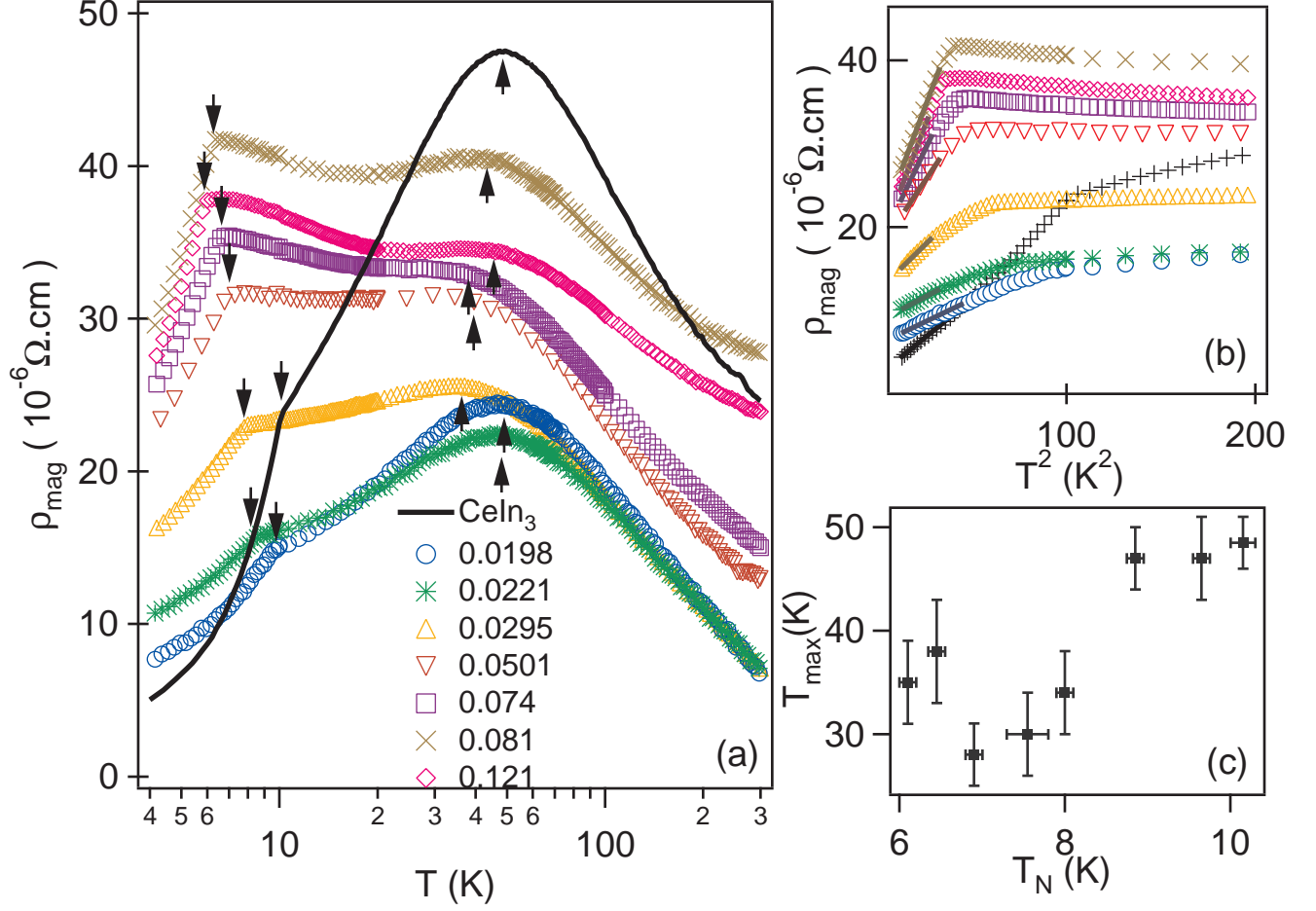


FIG. 6: (Color Online) (a) Magnetic contribution to the resistivity (ρ_{mag}) vs Temperature in the In-deficient single crystals of $\text{Ce}(\text{In}_{1-x}\text{Cd}_x)_{2.6}$, in the range 4 – 350 K on a semi-log scale at zero applied magnetic field. The Cd concentrations as determined from EDS are indicated. Up and down arrows indicate the position of the maximum in ρ_{mag} (at T_{max}) and of the AFM transition (at T_N), respectively. The magnetic contribution is obtained by subtracting the phonon contribution: $\rho_{mag} = \rho - \rho_{LaIn3}$. (b) ρ_{mag} vs Temperature squared (T^2) for the same samples. The solid lines correspond to the Fermi Liquid fits of the form $\rho_0 + AT^2$. (c) Coherence temperature T_{max} vs Neel temperature T_N with error bars, determined graphically from $\rho_{mag}(T)$.

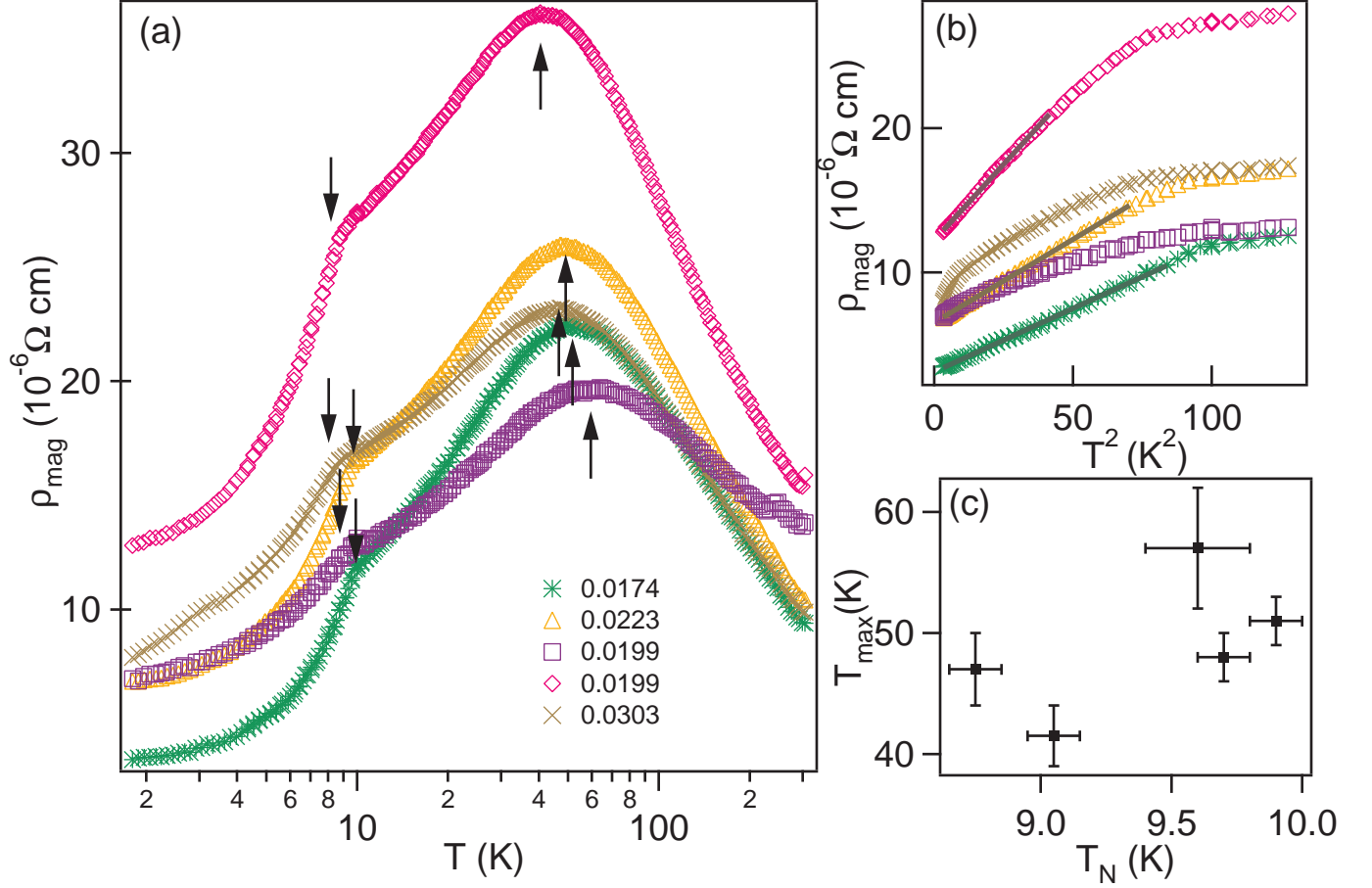


FIG. 7: (Color Online) (a) Magnetic contribution to the resistivity (ρ_{mag}) vs Temperature in the stoichiometric single crystals of $\text{Ce}(\text{In}_{1-x}\text{Cd}_x)_3$ between 1.8 – 300 K on a semi-log scale at $H = 500$ G applied magnetic field. The Cd concentrations as determined from EDS are indicated. Up and down arrows indicate the position of the maximum in ρ_{mag} (at T_{max}) and of the AFM transition (at T_N), respectively. The magnetic field ensures that free In inclusions are in the normal state. (b) ρ_{mag} vs T^2 for the same samples. The solid lines correspond to the Fermi Liquid fits of the form $\rho_0 + AT^2$. (c) Coherence temperature T_{max} vs Neel temperature T_N with error bars, determined graphically from $\rho_{mag}(T)$.

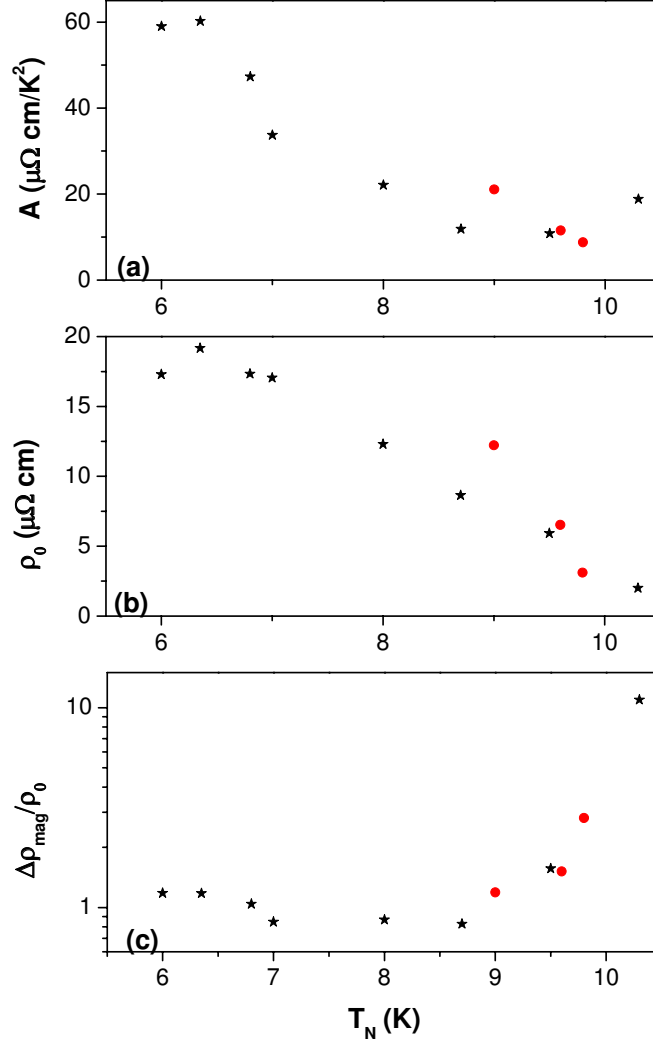


FIG. 8: (Color Online)(a)Fermi Liquid A coefficient of resistivity vs Neel Temperature in the In deficient (\star , $y = 2.6$) and stoichiometric (\bullet , $y = 3$) single crystals. (b) Residual Resistivity vs Neel Temperature in the same crystals. These parameters are obtained from fits to ρ_{mag} vs T^2 at the lowest temperatures, as indicated in Figures 6 and 7. (c) Normalized jump in the magnetic resistivity vs Neel Temperature on a semi-log plot for the same samples. The jump is defined as $\frac{\Delta\rho_{mag}}{\rho_0} = \frac{\rho(T_N) - \rho_0}{\rho_0}$ and is due to the suppression of spin-disorder scattering in the AFM state.